EUROPEAN ORGANIZATION FOR NUCLEAR RESEARCH

CERN-EP / 2000-108
July 20, 2000

NEW DEVELOPMENTS IN GASEOUS DETECTORS

Fabio Sauli

CERN, Geneva, Switzerland

Invited lecture at the
XXVIII International Meeting on Fundamental Physics
Sanlúcar de Barrameda, Cadiz, Spain 14-18 February 2000

NEW DEVELOPMENTS IN GASEOUS DETECTORS

FABIO SAULI

EP Division, CERN, CH-1211 Geneva, Switzerland
e-mail: fabio.sauli@cern.ch

The introduction in the late sixties of the multiwire proportional chamber initiated a very active and fruitful period of development and use of fast gas detectors. Exploiting various aspects of the signal formation and amplification, performing position-sensitive devices have been developed and used in particle physics, medical diagnostics, biology, astrophysics. A fundamental rate limitation of wire chambers, due to positive ion accumulations, was overcome with the micro-strip gas chamber, capable of achieving position accuracy of few tens of microns at radiation fluxes exceeding a MHz/mm^2. Two problems however emerged: a slow degradation under sustained irradiation (aging), and a rarer but destructive appearance of discharges. New breeds of detectors, aimed at improving on these crucial points, have been introduced and intensively studied: microdot, CAT, micromegas, gas electron multiplier are representative examples. Very performing, they appear to be more robust and reliable. Multi-stage devices, making use of a gas electron multiplier as pre-amplifying elements, permit to sustain larger gains in presence of high rates and heavily ionizing tracks. The progress made in the field leads to new concepts in gas detectors, powerful yet cheap and reliable.

1 Basic processes in gaseous detectors

The process of detection in gas proportional counters begins with the primary ionizing interaction between particles and gas molecules and the release of electron-ion pairs. The amount n_P and the space distribution of the primary ionization depend on the nature and energy of the radiation. The primary electrons can have enough energy to further ionize the gas molecules, generating local clusters of charge; the overall number of pairs (primary and secondary) is called total ionization, n_T. Charged particles release a trail of clusters, while photons undergo a single interaction, usually with the emission of a long-range electron. Table 1 provides, for minimum ionizing particles, relevant ionization parameters for some gases commonly used in proportional counters, at standard conditions. For different conditions, and for mixtures, simple scaling rules apply [1].

Table 1: Ionization parameters for several gases at STP

Gas (STP)	Density g cm^{-3}	dE/dx keV cm^{-1}	*W* eV	n_P pairs cm^{-1}	n_T pairs cm^{-1}
Helium	$1.7\ 10^{-4}$	0.32	41	6	8
Argon	$1.7\ 10^{-3}$	2.4	26	25	94
Xenon	$5.5\ 10^{-3}$	6.8	22	44	307
Methane	$6.7\ 10^{-4}$	1.5	28	16	53
Carbon dioxide	$1.9\ 10^{-3}$	3.0	33	35	91

In the table, the quantity *W* represents the average energy required per ion pair, and is almost an invariant for each gas in a wide range of particles and energies. As an example, the total number of pairs created by a 5.9 keV X-ray totally absorbed in argon is ~ 220 (5900 / 26).

The primary statistics determines several intrinsic performances of detectors, such as efficiency, time resolution and localization accuracy. The actual number of primary interactions follows the Poisson's law; the inefficiency of detection of a thin layer of gas is given by $\exp(-n_p)$. For example, in one mm of argon about 8% of all minimum ionizing tracks do not release a single cluster, and are therefore not detected. The total ionization loss, sum of primary and secondary ion pairs, follows a statistical distribution described by a Landau function, with characteristic tails towards high values (Fig. 1). This is essentially due to the appearance of rare but energetic electrons ejected in some encounters, named delta electrons.

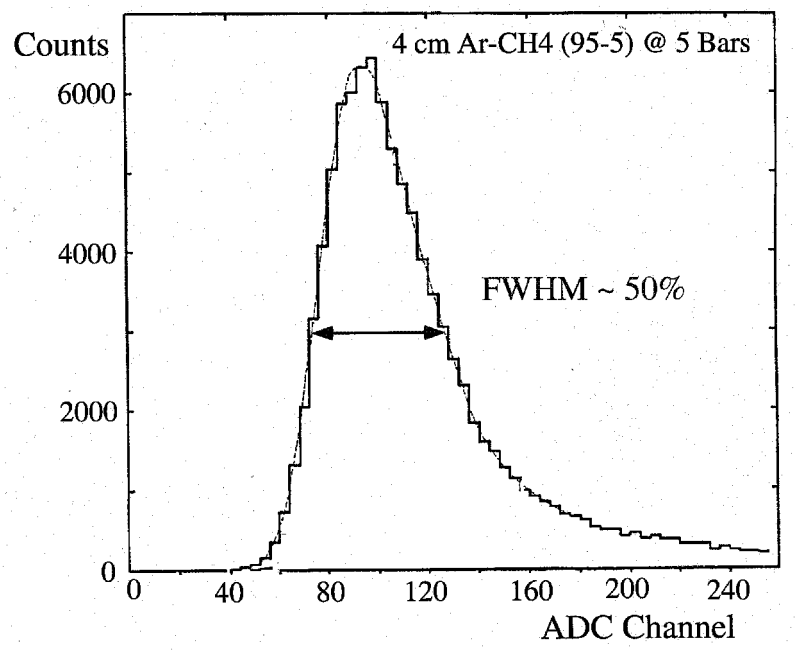

Figure 1: Distribution of ionization loss for fast particles in thin layers of gas.

Once released in the gas, ions and electrons diffuse by collision with the surrounding molecules. At room temperature, it takes a few seconds for an initially point-like charge concentration to evolve into a cloud several mm wide. This explains the rapid dilution of pollutants in a closed gas envelope, and the fast spread over all the counter of contaminants due to leaks. Direct charge recombination or neutralization at the walls eventually eliminates the ions.

When an external electric field is applied, a collective motion of charges overrimposes to the thermal diffusion; the average distance reached by the cloud divided by the time is called drift velocity. For ions, the drift velocity is proportional to the field, and their ratio, called mobility, is roughly constant. Typical values of mobility for several ions are given in Table 2 [2, 3]. It can be seen for example that in field values typically used in gas detectors, around one kV cm^{-1}, it takes to argon ions 200 μs to migrate along one cm. The mobility of ions in gas mixtures can be computed from simple composition laws.

Table 2: Ions mobility in their own gas at STP

ION	GAS	μ ($cm^2V^{-1}s^{-1}$)
He^+	He	10.2
Ar^+	Ar	1.5
CH_4^+	Ar	1.87
CH_4^+	CH_4	2.26
CO_2^+	CO_2	1.09

Electrons easily acquire energy from the external field; since the electron-molecule collision cross section depends on energy, in a peculiar way for each gas, the drift velocity evolves very differently with the field in different gases and mixtures. Fig. 2 shows this behavior in several pure gases; given the value of field, the drift velocity can vary over an order of magnitude. The behavior in mixtures is even more complex; it can be computed [4] or obtained from dedicated compilation works [5]. Typically, in gases used in proportional counters and at fields around one kV cm^{-1}, the electron drift velocity is around 5 cm μs^{-1}, and the corresponding drift time 200 ns cm^{-1}, one thousand times faster than ions in the same field.

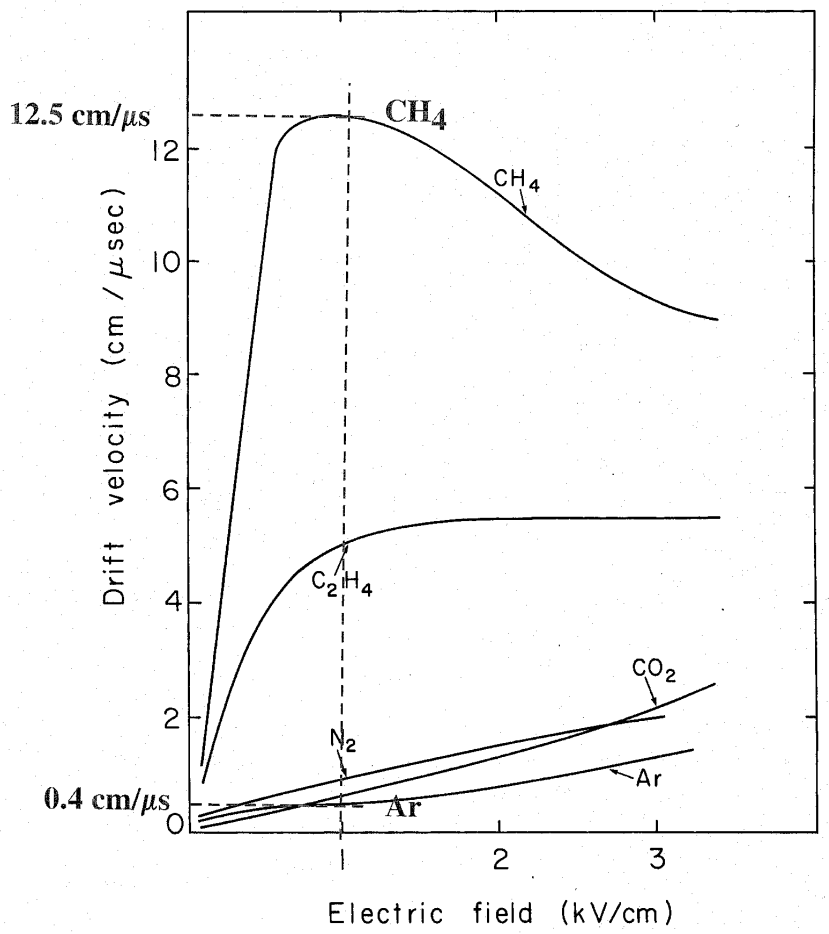

Figure 2: Electron drift velocity in various gases at STP.

The electron diffusion as a function of field also depends from the energy dependence of the collision cross sections involved. Fig. 3 gives examples of the single electron rms diffusion, for one cm of drift, in several gases at STP [6]. Given the value of field, the width of diffusion varies from few tens of microns to several mm. The dispersion of the original charge cloud before collection at the electrodes determines the localization properties of detectors.

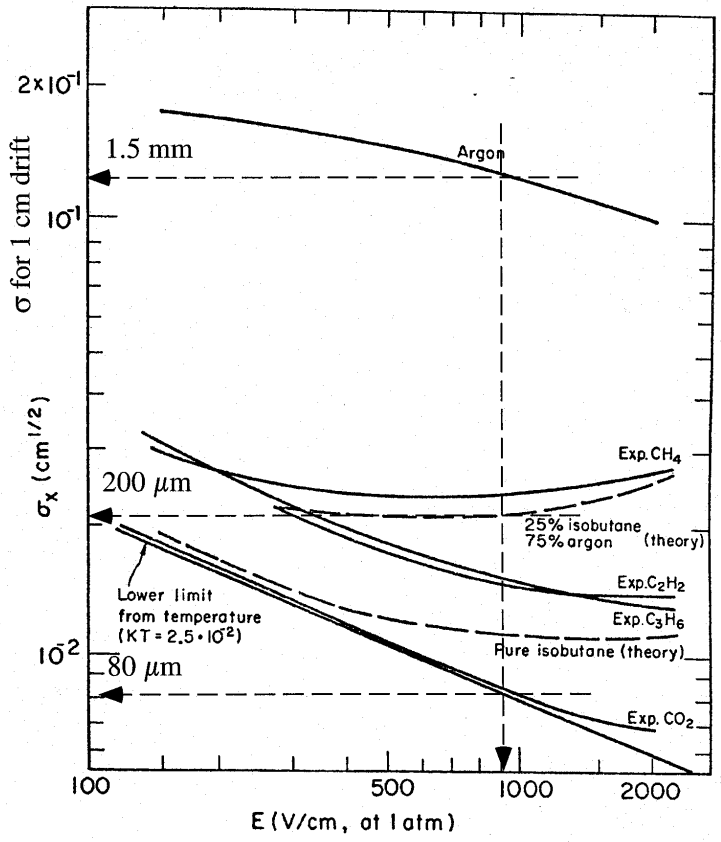

Figure 3: Single electron space diffusion per cm of drift in various gases at STP.

If the electric field is increased above a critical value (a few to a few tens of kV cm^{-1}, depending on gas), electrons begin to experience inelastic collisions with the molecules. Reaching an energy above the ionization potential, they can generate of a new electron-ion pair. This defines for each gas a field-dependent ionization mean free path λ; its inverse, α, is named the first Townsend coefficient. Fig. 4 gives some examples of fast increase of the Townsend coefficient (actually of α / P, P being the gas pressure) from the reduced field E/P [7]. New ionizing collisions develop at each mean free path, growing an avalanche of charge with the fast electrons in the front and the much slower ions left behind. In uniform field the avalanche size, started by one electron, after a path x is given by $\exp(\alpha x)$; this defines the gain of the counter. For the more general case of non-uniform field the avalanche size can be obtained by integration, insomuch as the field dependence of the Townsend coefficient is known.

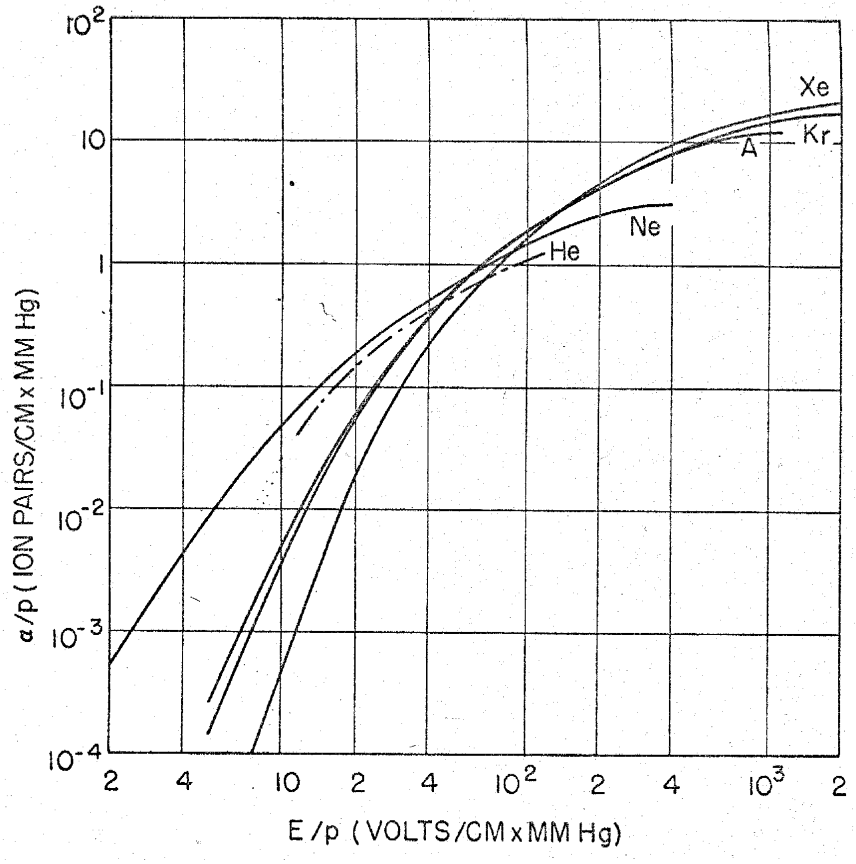

Figure 4: First Townsend coefficient in noble gases.

In the proportional counter, the electric field increases only in the vicinity of the thin anode wire, where multiplication occurs; the charge released in most of the counter's volume is therefore amplified by a fixed factor, hence the name proportional. Fig. 5 shows the dependence of detected charge from operating voltage in a typical single wire counter. After an initial plateau of simple collection (the ionization chamber region), the signal increases exponentially, with an amplitude that depends from the original ionization charge. At very high voltages, however, the proportionality is gradually lost, and the counter enters a regime of saturated response or discharge. Particularly interesting for what follows is the observation of a transition, at high gains, from a proportional to a streamer multiplication (Fig. 6 [8]). This is observed to occur in most counters with thin anodes and operated at atmospheric pressure in well quenched gases. As seen in the figure, the onset of the transition depends on the density of the ionizing trail; the total charge at the transition is roughly constant, the so-called Raether limit.

The motion and collection of charges induces detectable signals on all electrodes of the detector. For a thin wire proportional counter, after a small and very fast signal generated by the collection at the anode of the electrons, most of the detected signal is due to the retrograde motion of positive ions produced in the avalanche. The total signal length corresponds then to the collection time of positive ions, several hundred μs as said before. For most applications, the signal is heavily differentiated to extract its fast component, as shown in Fig. 7.

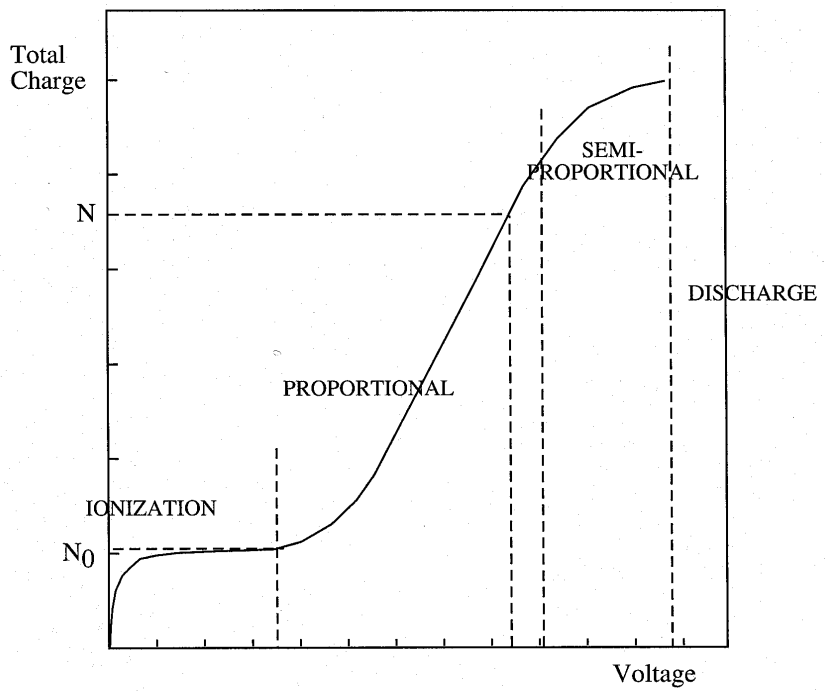

Fig. 5: Charge-voltage characteristics of a proportional counter.

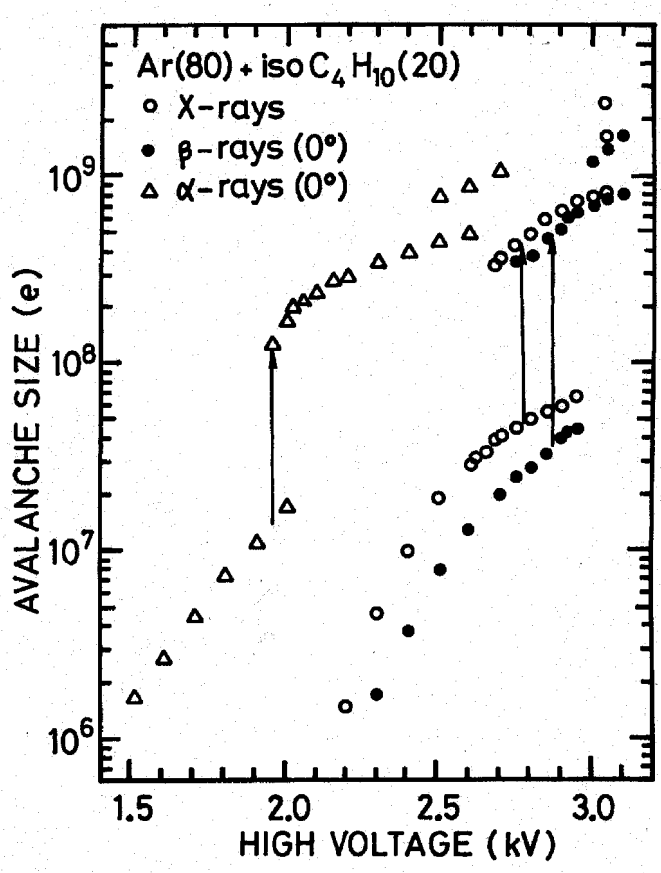

Figure 6: Transition from proportional avalanche to streamer for several particles.

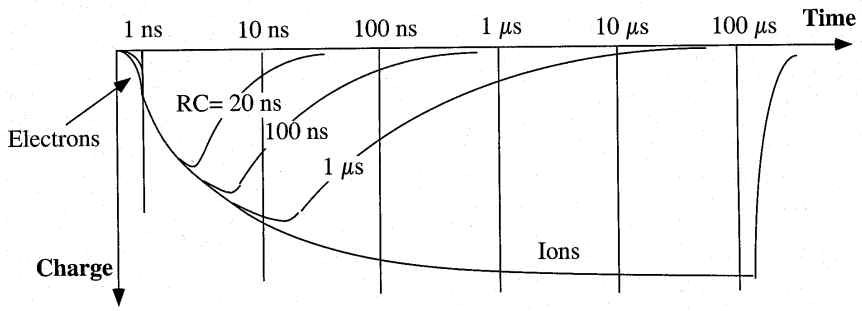

Figure 7: Signals in a proportional counter for several shaping constants.

2. Multiwire Proportional Chambers and derivatives

The invention of the Multi-Wire Proportional Chamber (MWPC) revolutionized the field of radiation detectors [9]. In its basic configuration, the MWPC consists of a set of thin, parallel anode wires stretched between two cathode planes; application of symmetric potentials between anodes and cathodes creates the field structure shown in Fig. 8. Electrons released by ionization in the gas drift towards the anodes and, approaching the thin wires, multiply in a proportional avalanche. With anode and cathode wire planes segmented, and recording the induced signals on electrodes, MWPCs allow determining the avalanche position with sub-millimeter accuracy; this two-dimensional localization capability is fundamental in imaging applications [10].

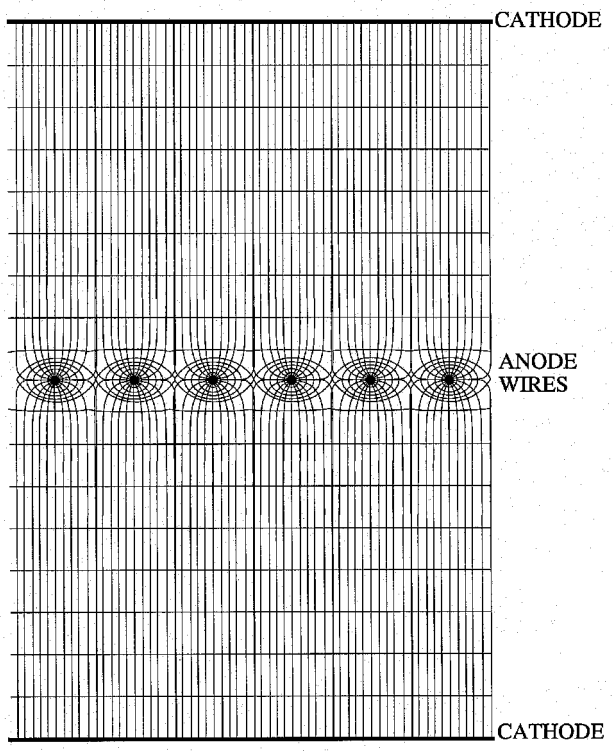

Figure 8: Schematics and electric field of the MWPC.

Many descendants of the MWPC, with novel geometry and exploiting various gas properties, have been developed and extensively used: drift, time projection, ring imaging chambers are representative examples. With their excellent position accuracy and rate capability, they still constitute a major tool in particle physics experiments .[11-13].

Wire proportional counters suffer from an intrinsic limitation: at high radiation rates, the production of slow positive ions results in the build-up of a space charge, interfering with the counting action. In standard operating conditions, the gain of a MWPC begins to drop at rates above 10^4 mm^{-2}s^{-1}, quickly leading to a loss of detection efficiency (Fig. 9). Together with the practical difficulty to manufacture detectors with sub-mm wire spacing, this has motivated the development of a new generation of devices to cope with the demanding needs of the new generations of high luminosity accelerators.

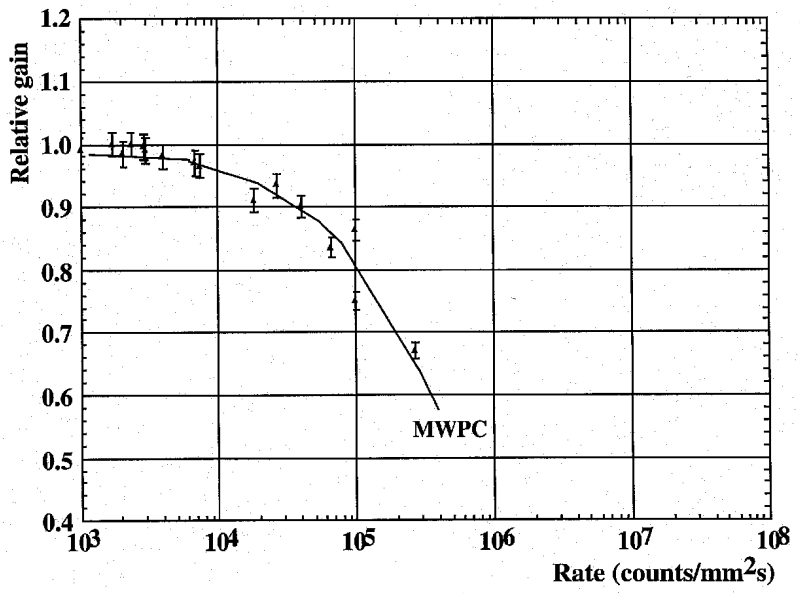

Figure 9: Gain reduction with rate induced by positive ions accumulation in the MWPC.

3. Micro-Strip Gas Chambers

The micro-strip gas chamber (MSGC [14]) improves the rate capability by more than an order of magnitude. Thin, metallic parallel strips are laid on an insulating support; connected alternatively to positive and negative potentials, the strips act as a multi-anode proportional counter (Fig. 10). The small distance between strips typically 100 µm, ensures a fast clearing of the ions produced. For operation at high rates, in order to avoid the accumulation of ions in the interstice between strips, slightly conducting supports are used: semi-conducting or surface-treated glass. Fig. 11 shows an example of rate capability of a MSGC plate manufactured on a glass support coated with a thin diamond-like resistive layer [15]. The intrinsic position accuracy of MSGC, measured for soft X-rays, is of around 30 µm rms, obtained recording the charge on strips and computing its center of gravity. In detecting charged particles, the position accuracy depends from the incidence angle, as shown in Fig 12, a consequence of the primary ionization statistics [16].

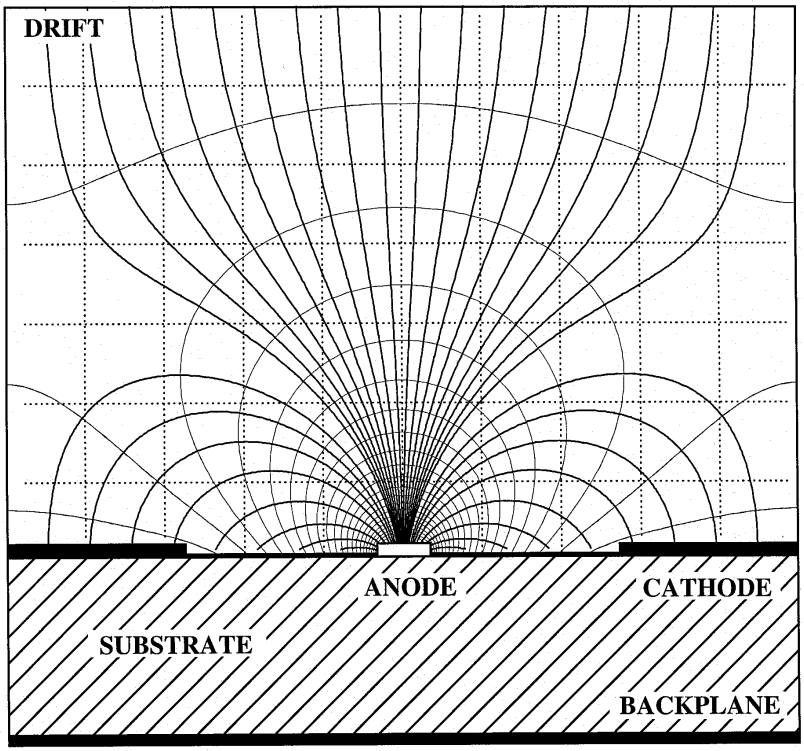

Figure 10: Schematics and electric field of the MSGC.

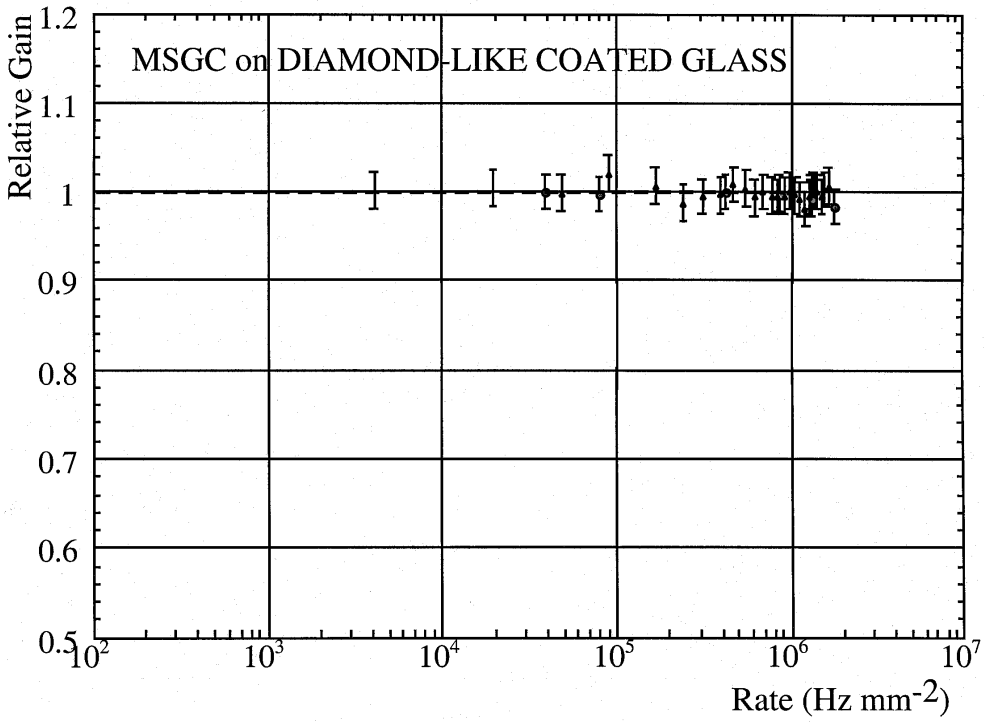

Figure 11: Relative gain as a function of flux for a MSGC made on diamond coated glass.

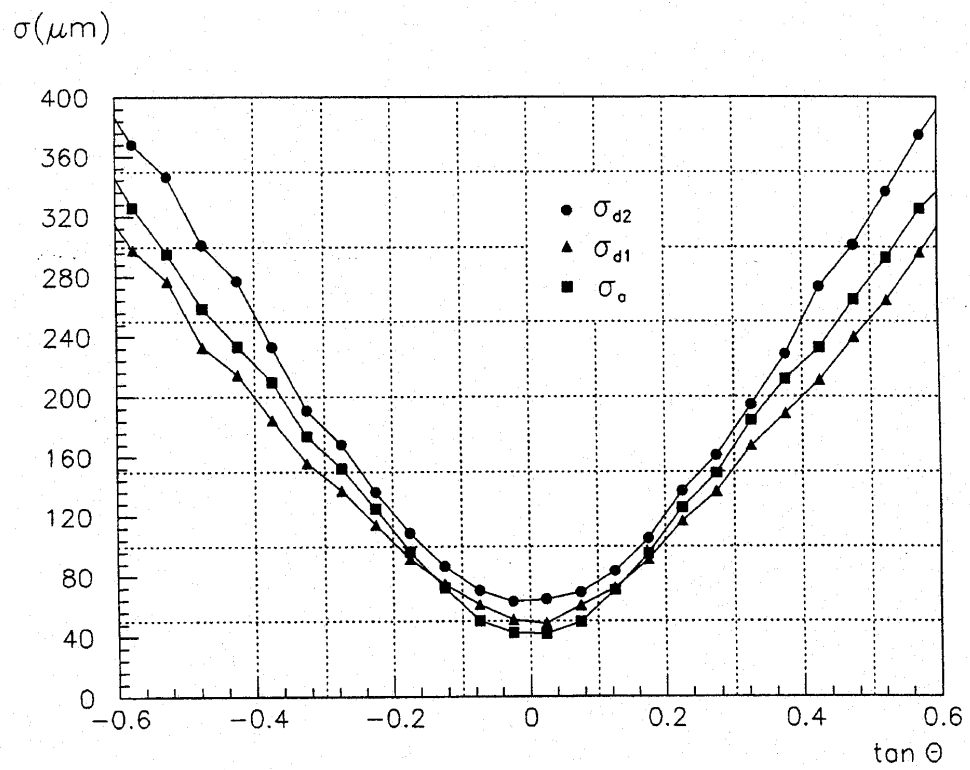

Figure 12: Position accuracy of the MSGC as a function of the track's angle to the normal.

Developed by many groups, and intended for use in major experiments for the new high luminosity colliders, MSGCs appeared however rather susceptible to aging and discharge damages. Long-term studies have revealed a slow degradation of performances, attributed to the formation of polymers in the avalanches. MSGCs are particularly prone to aging because of the small electrode area; minute amounts (few ppm) of organic pollutants released by materials or in the gas flow strongly affect the detector lifetime. With proper choice of the components, a long-term survival up to a collected charge above 100 mC per cm of strip has been demonstrated, equivalent to ten years of operation at LHC [17].

The appearance of destructive discharges appeared instead to be a more serious problem, and an unavoidable consequence of the presence, in the field of particles to be detected, of rare but heavily ionizing tracks (nuclear fragments, gamma and neutron conversions). As discussed in the first section, this can lead to a transition of the avalanche to a streamer, followed by a discharge [18]. Fig. 13 illustrates the basic problem [19]. As a function of voltage, it provides the proportional gain and the efficiency plateau for minimum ionizing particles, for a typical configuration and making use of currently available high-density electronics. For full efficiency, a minimum gain around 2000 has to be reached. Exposing the detector to alpha particles, one observes a fast increase of the discharge probability as a function of voltage, as shown in the figure; it clearly indicates the marginality of operation of the detector. Moreover, laboratory measurement may be optimistic both in rate and ionization losses as compared to realistic beam operating conditions, as found by the group developing a fast tracker for HERA-B, that led to abandon the MSGC technology [20].

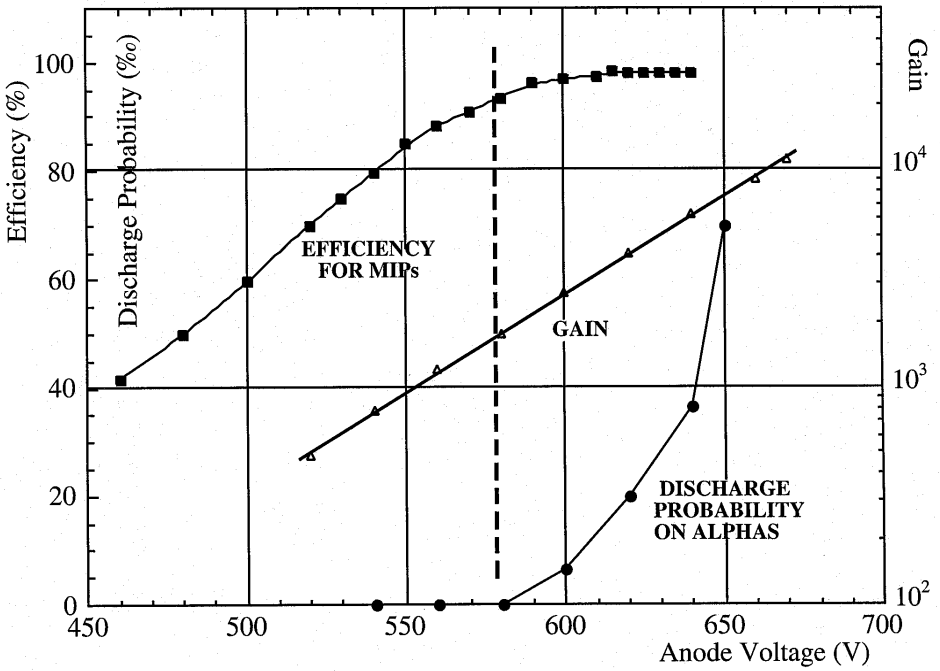

Figure 13: MSGC gain, efficiency for minimum ionizing tracks and discharge rate on exposure to alpha particles as a function of voltage.

4 Recent developments: CAT, Micromegas, GEM, Microwire Chambers

Motivated by the problems mentioned above, a large effort has been devoted to find more rugged alternatives to the MSGCs, without compromising on their performances. At the same time, detailed studies have shed new light on the transition and discharge mechanisms. The new class of devices, named Micro-Pattern Detectors (MPD), brings very promising perspectives of applications.

A very interesting device is the so-called "Compteur à Trous" or CAT [21]. It consists of a matrix of holes, drilled through a metallic foil with an anode at the bottom (Fig. 14). Proportional gains up to 10^4 and good energy resolution have been demonstrated. Several variations of the CAT structure have been developed, with multiple holes and an insulator plate between anode and cathode in order to improve the mechanical stability and easy the construction; the charge transport properties have also been studied with the help of analytical calculations [22]. Large area detectors, named micro-CAT, have been developed specifically for the use in medical imaging. In this case, good two-dimensional localization accuracy is obtained measuring the charge sharing on a resistive anode [23].

Micromegas, a thin-gap parallel plate counter, is shown schematically in Fig. 15 [24]. It consists of a thin metal mesh, stretched above a readout electrode, at a distance of 50 to 100 μm. Regularly spaced supports (insulating fibers or pillars) guarantee the uniformity of the gap. A high field is applied across the multiplying gap, and electrons released in the upper drift region are collected and multiplied. Operation at very high particle fluxes has been demonstrated, with good efficiency plateaus for minimum ionizing particles [25]. Recently, very good localization properties have been demonstrated making use of low diffusion gases [26].

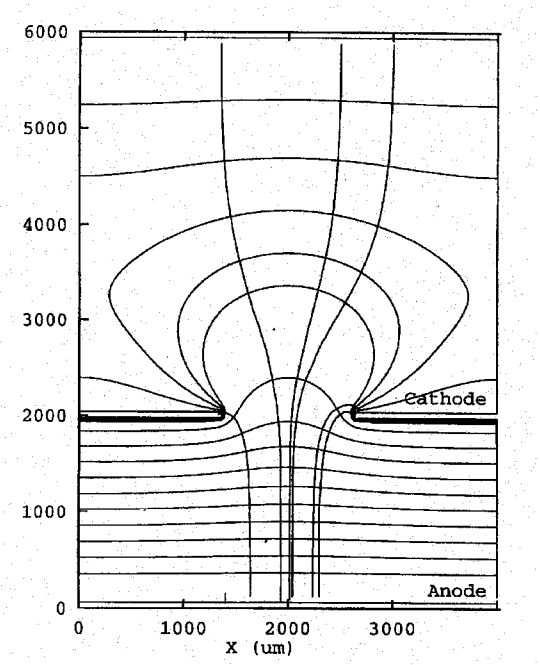

Figure 14: Schematics of the CAT detector.

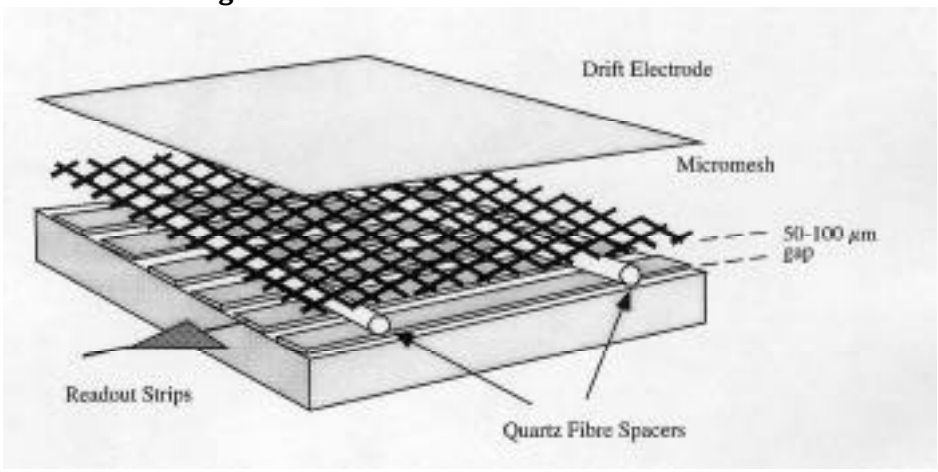

Figure 15: Schematics of the Micromegas.

The Gas Electron Multiplier (GEM) is another innovative multiplying structure [27]. It consists of a metal-insulator-metal thin-foil composite, chemically pierced with a high density of holes, typically 50-100 μm in diameter at 100-200 μm pitch. With proper choice of potentials, electrons released in the gas above the foil are drifted into the holes, and multiplied in avalanche in the high field within the channels (Fig. 16). Most of the electrons in the avalanche move into the lower gap and are collected; effective gains well above several thousand can be achieved, sufficient for detection of minimum ionizing tracks in thin conversion layers. Localization can then be performed collecting the charge on a patterned one- or two-dimensional readout board [28]. A unique feature of GEM detectors is that proportional multiplication and charge detection are performed on separate electrodes; with proper choice of the operating conditions one can effectively avoid the propagation of discharges to the sensitive electronics.

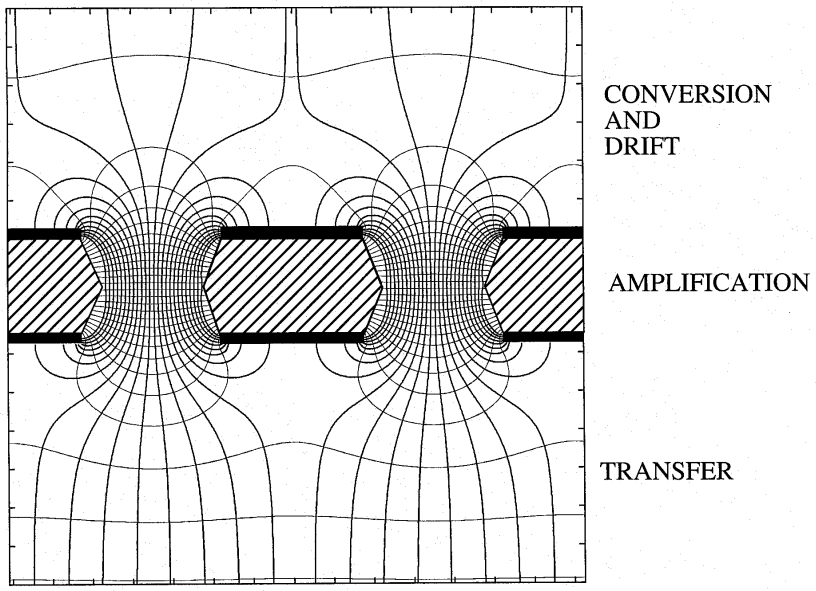

Fig. 16: Schematics and field in the GEM detector.

Exploiting the kapton-etching technology developed for making GEM electrodes, other promising multiplying structures have been recently developed: the micro-groove (Fig. 17) [29] and the micro-wire detector (Fig. 18) [30]. All devices permit to reach gains above 10^4.

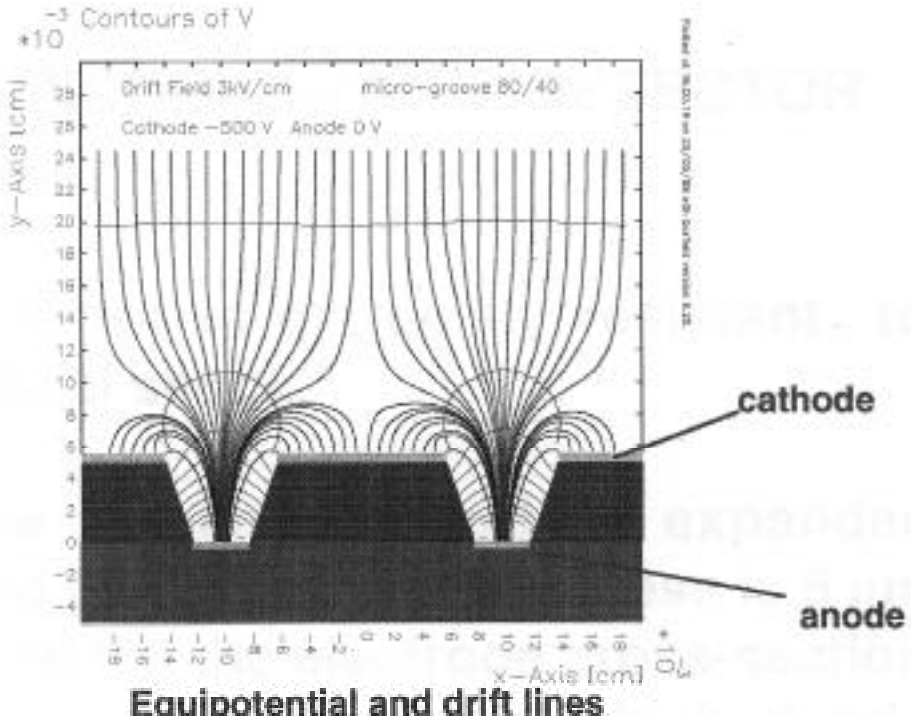

Figure 17: Schematics of the micro-groove detector.

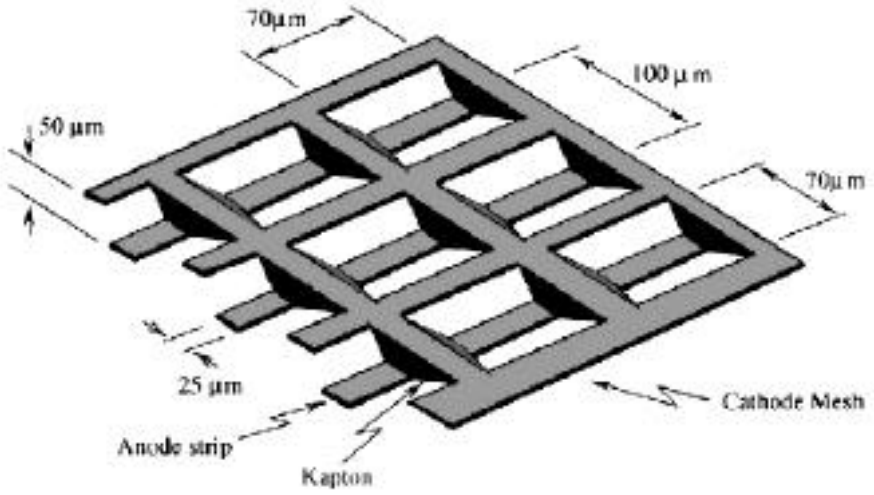

Figure 18: The micro-wire detector.

Recent measurements have shown that MPD structures, similarly to the MSGC, exhibit a fast increasing discharge rate with voltage when exposed to high rates or highly ionizing alpha particles [31, 32]. They have therefore a similar limitation in gain, although the sturdier construction prevents permanent damages to the electrodes under repeated discharges. As an example, Fig. 19 shows the behavior of the Micromegas detector; within a factor of two, the gain at the discharge threshold is the same as for the MSGC (see Fig. 13). The appearance of discharges is attributed to the avalanche size exceeding a critical value, in the range 10^7-10^8 (the so-called Raether limit); the ensuing field distortion induces a spontaneous, photon-mediated transition from a proportional avalanche to a streamer. In MPDs, having a rather high field over small distances, a further transition from streamer to discharge is very likely to occur.

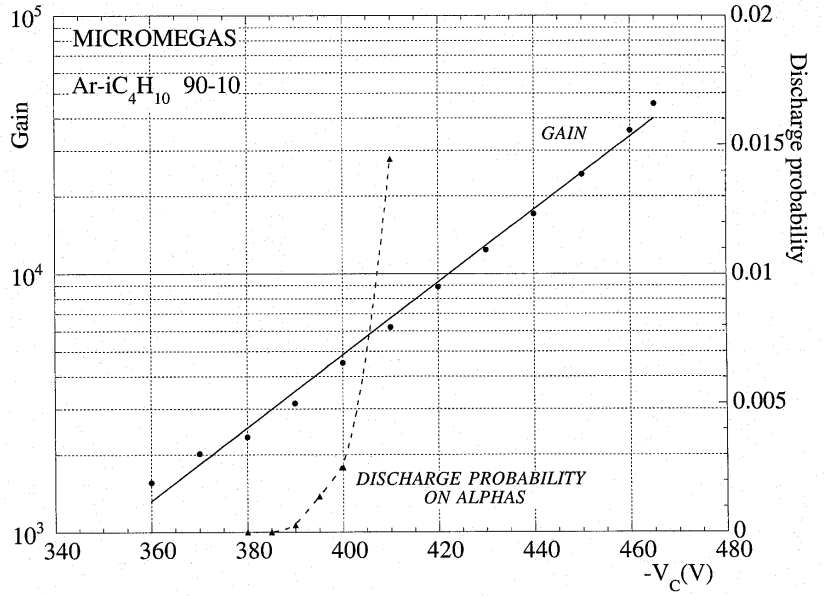

Figure 19: Gain and discharge rate on alphas for Micromegas.

A similar reduction in maximum gain has been observed exposing the detectors to increasing fluxes of X-rays. In this case, it is not very clear however how the total avalanche charge can reach the limit, unless one invokes the presence of long-lived excited states or surface charge accumulations followed by spontaneous emission [32, 33].

A solution to this fundamental problem has been found cascading several multiplying elements, an approach developed long ago in the so-called Multistep Chamber [34]. This can be easily achieved with the GEM, used as a pre-amplifier in combination with another MPD. With a GEM in front of a MSGC, the two-stage detector permits to reach much higher gains before discharge, or alternatively to operate at a given gain with each element at much reduced voltage and therefore in a much safer condition (Fig. 20) [35]. This is the solution adopted for the above mentioned HERA-B experiment, and has led to the first large production of GEM electrodes: more than two hundred foils, 27x25 cm^2 each, have been manufactured at CERN [36]. Fig. 21 shows the gain and discharge rates measured with the double structure; comparison with Figs. 13 shows the substantial increase of the operational margin . The detectors are at present being installed at DESY.

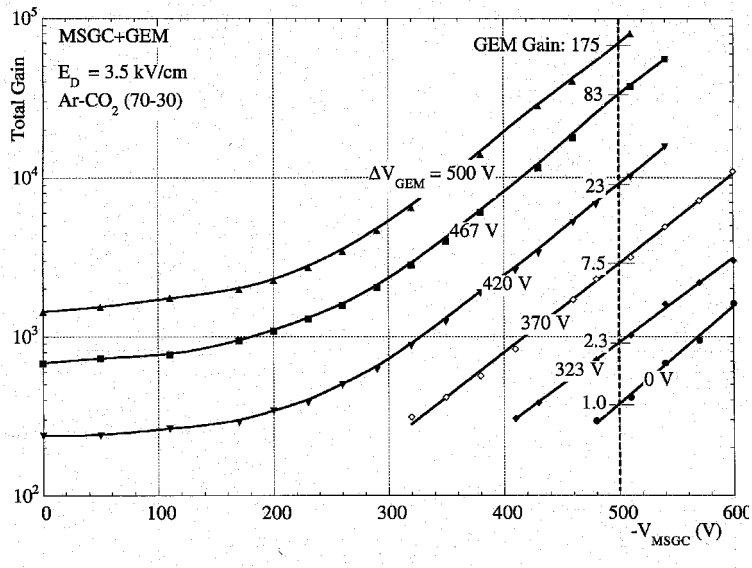

Figure 20: Combined gain as a function of voltages of the MSGC+GEM detector.

Similar performances are obtained with multiple GEM devices, intrinsically cheaper and more robust than MSGCs [37]. Double GEM detectors (Fig. 22) have been extensively tested in particle beams [38], and three and four-stage GEMs are under development to obtain higher safe gains and single photoelectron detection. With a double GEM, gains in excess of 10^4 can be reached at very high rates, see Fig. 23. The discharge boundary on irradiation with alpha particles is plotted as a function of gain for a double GEM in Fig. 24 [31]. The maximum safe gain is about an order of magnitude larger than for a single structure. The exact reasons for the improvement are not completely clear. It is suspected that, since in cascaded system the same overall gain is obtained with each element operated at much reduced voltage, the amount of charge required for the transition is larger. In other words, the Raether limit is voltage dependent. Alternatively, one can invoke the larger avalanche spread in multiple structures to reduce the charge density.

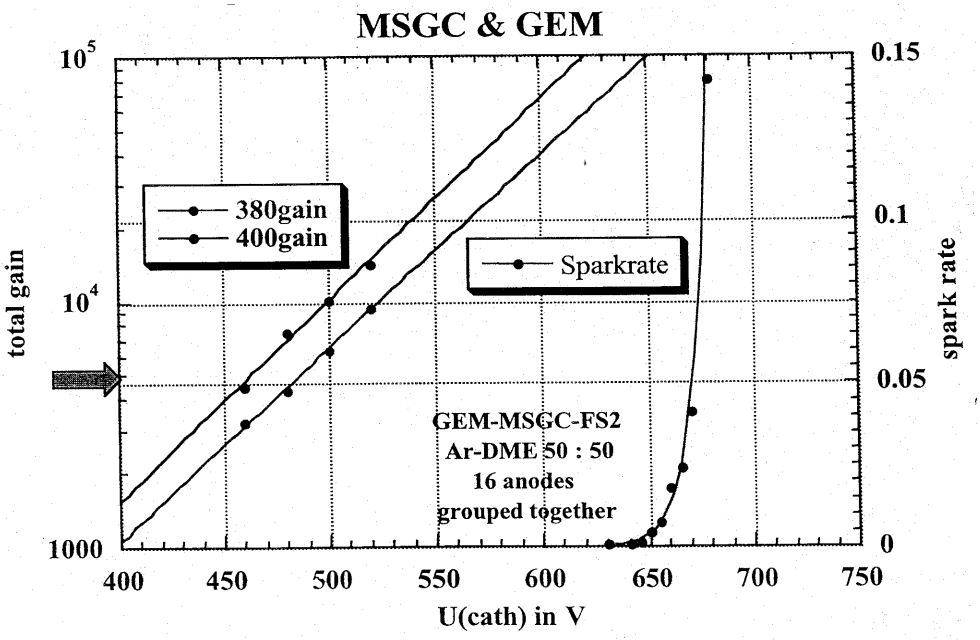

Figure 21: Gain and discharge rate in the HERA-B MSGC+GEM detector.

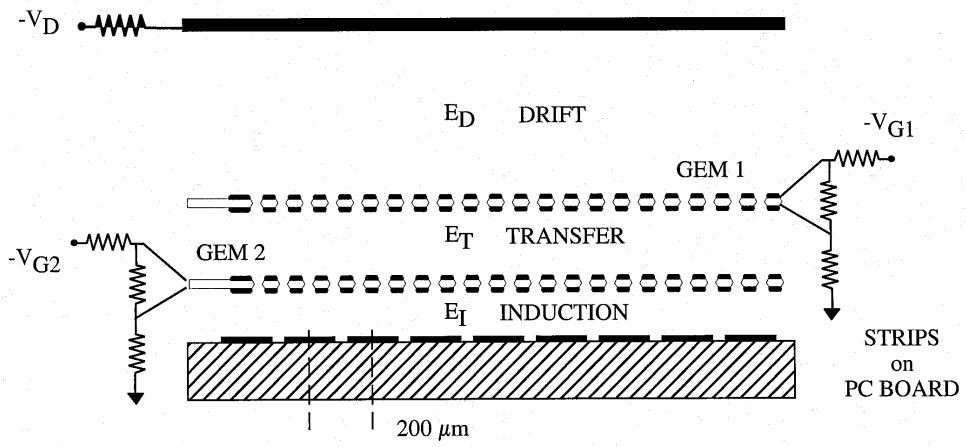

Figure 22: Schematics of the Double GEM detector.

A set of large size (31x31 cm^2 active) double-GEM detectors is in construction at CERN for the needs of the COMPASS experiment; prototypes have been successfully tested in realistic experimental conditions [39]. Fig. 25 shows one detector installed in a high intensity beam at the Paul Sherrer Institute.

GEM detectors can be easily equipped for two-dimensional read-out, sharing the collected electrons in the last gap between two sets of perpendicular strips; this is the solution adopted for the COMPASS chambers. Exploiting the signal detected on the lower electrode of the GEM closer to the read-out board, one can trigger the charge recording electronics on neutral events and realize two-dimensional maps of X-ray activity [28]. Fig. 26 gives an example of X-ray absorption radiography of a small mammal, recorded with a double GEM detector; the image size is about 6x3 cm^2. The intrinsic space resolution is better than 100 μm, a promising feature for possible medical applications.

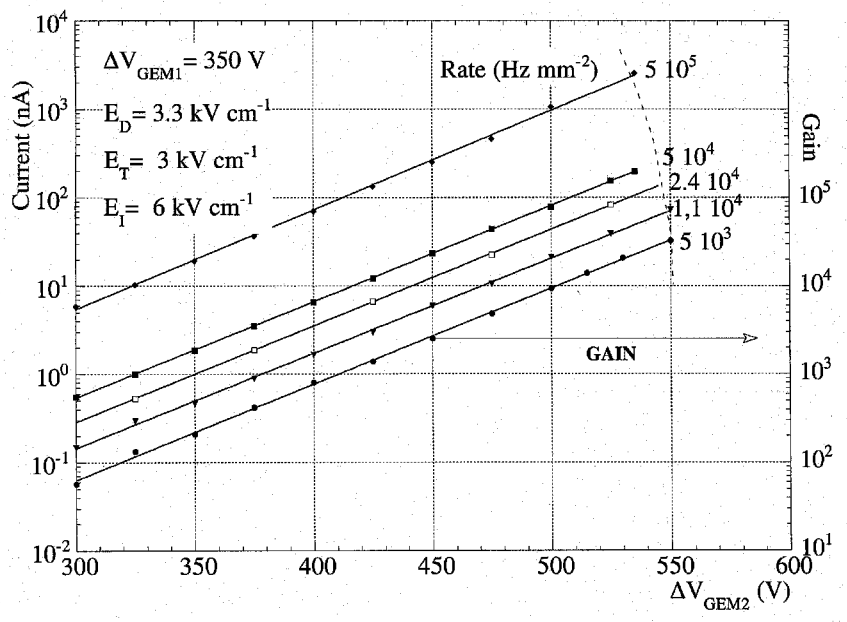

Figure 23: Current measured at increasing X-ray fluxed in the Double GEM. For the lower curve the corresponding gain can be read on the right scale.

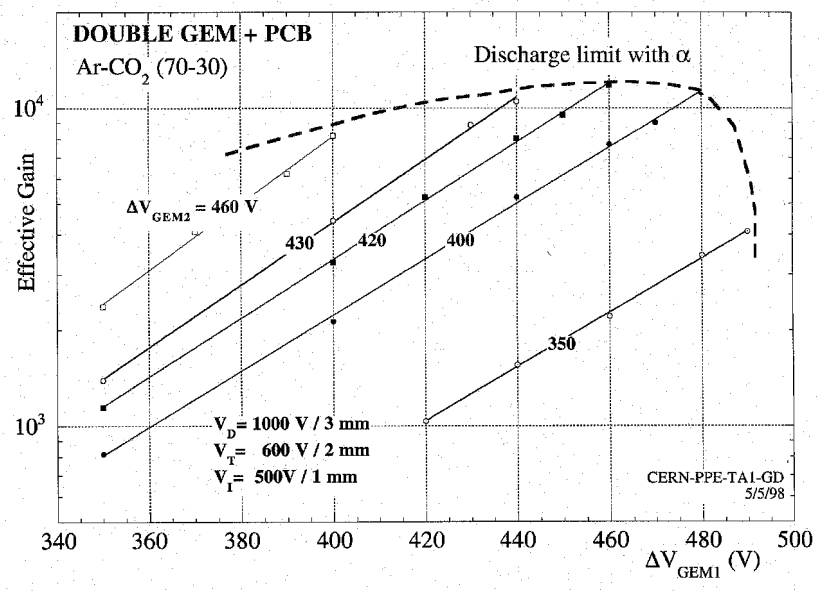

Figure 24: Discharge boundary as a function of voltage sharing between the two GEMs.

The confinement of avalanches in the holes, with the consequent suppression of photon feedback, probably explains the exceptionally large gains obtained operating the device in pure argon, see Fig. 28 [40]; applications include the development of sealed counters. A very attractive possibility is to use the upper GEM electrode, facing a transparent window, as photocathode, followed by a transfer of the photoelectrons through the holes to a following gas amplifying device. The strong suppression of photon and ion feedback in this reverse photocathode configuration should permit to obtain efficient single photon detection; various gain-limiting feedback processes are being analyzed in order to optimize the device [41].

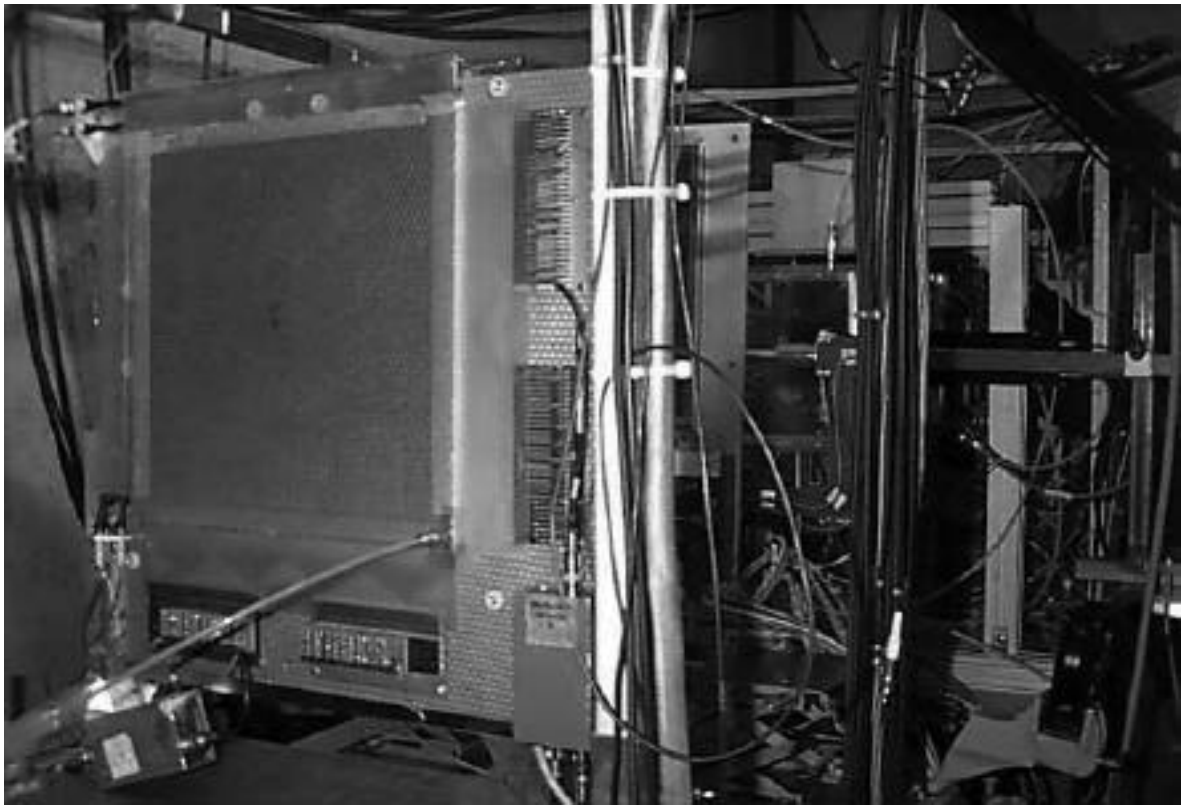

Figure 25: A large Double GEM prototype for COMPASS tested in the PSI beam.

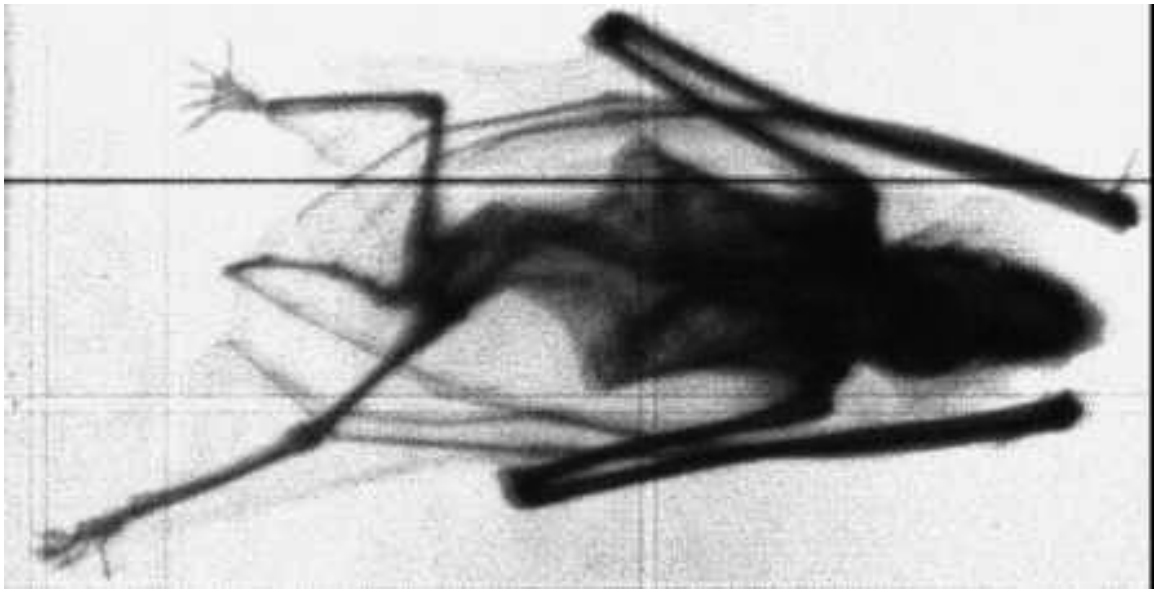

Figure 26: X-Ray absorption radiography of a small bat recorded with a Double GEM.

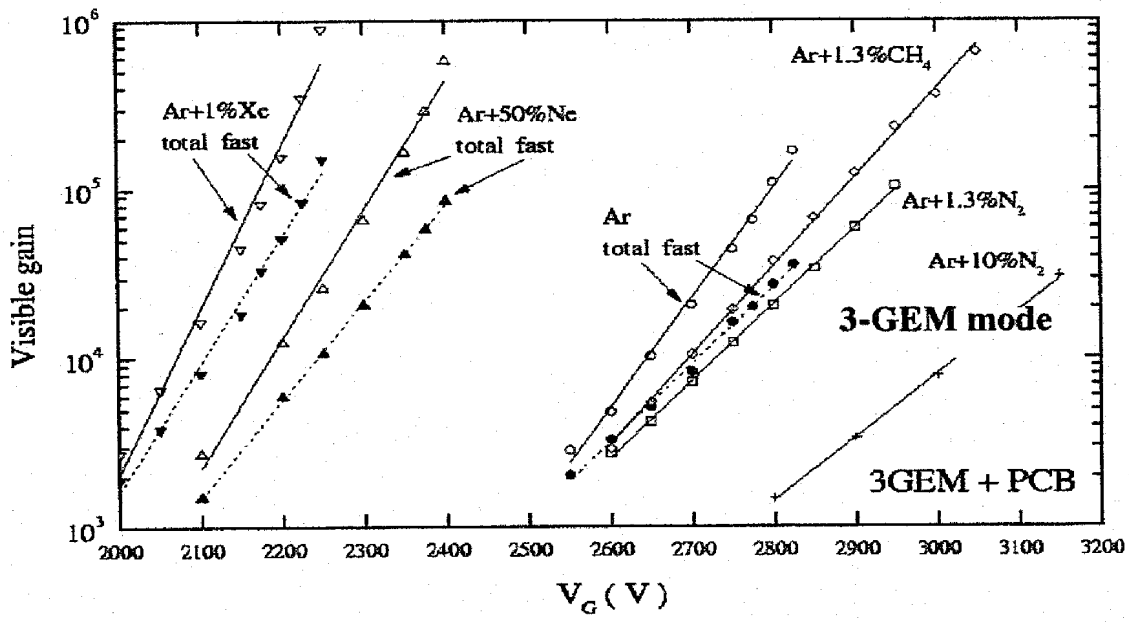

Figure 27: Gain as a function of voltage measured with a Triple GEM detector in several gas mixtures.

References

[1] F. Sauli, CERN 77-09 (1977).
[2] E.W. McDaniel *et al.*, The mobility and diffusion of ions in gases (Wiley & Sons, New York 1973).
[3] G. Schultz *et al.*, Rev. Physique Appliquée 12 (1977) 67.
[4] S.F. Biagi, Nucl. Instrum. and Meth. A 283 (1989) 716.
[5] A. Peisert *et al.*, CERN 84-08 (1984).
[6] V. Palladino *et al.*, Nucl. Instrum. and Meth. 128 (1975) 323.
[7] S.C. Brown, Basic data on plasma physics (MIT Press, 1959).
[8] N. Koori *et al.*, Jap. J. Appl. Phys. 25 (1986) 986.
[9] G. Charpak *et al.*, Nucl. Instrum. and Meth. 62 (1968) 262.
[10] F. Sauli, Nuclear Instr. and Meth. A422 (1999) 257.
[11] F. Sauli, New developments in gaseous detectors, *in* Techniques and concepts of high-energy physics, T. Ferbel, Editor (Plenum 1983) 301-350.
[12] C. Grupen, Particle Detectors (University Press, Cambridge 1996).
[13] F. Sauli, Nucl. Instrum. and Meth. A419 (1998) 189.
[14] A. Oed, Nucl. Instrum. and Meth. A263 (1988) 351.
[15] R. Bouclier *et al.*, Nucl. Instrum. and Meth. A 369 (1996) 328.
[16] F. van den Berg *et al.*, Nucl. Instrum. Methods A 349 (1994) 438.
[17] R. Bouclier *et al.*, Nucl. Instrum. and Meth. A381 (1996) 289.
[18] V. Peskov *et al.*, Nucl. Instrum. and Meth. A397 (1997) 243.
[19] R. Bouclier *et al.*, Nucl. Instrum. and Meth. A365 (1995) 65.
[20] B. Schmidt, Nucl. Instrum. and Meth. A 419 (1998) 230.
[21] F. Bartol *et al.*, J. Phys. III France 6 (1996) 337.
[22] G. Chaplier *et al.*, Nucl. Instr. and Meth. A426 (1999) 339.
[23] A. Sarvestani *et al.*, Nucl. Instrum. and Meth. A 419 (1998) 444.

[24] I. Giomataris *et al.*, Nucl. Instrum. and Meth. A376 (1996) 29.
[25] Y. Giomataris, Nucl. Instrum. and Meth. A 419 (1998) 239.
[26] J. Derré *et al.*, DAPNIA/00-03. Subm. Nucl. Instrum. Methods (2000).
[27] F. Sauli, Nucl. Instrum. and Meth. A386 (1997) 531.
[28] A. Bressan *et al.*, Nucl. Instrum. and Meth. A425 (1999) 254.
[29] R. Bellazzini *et al.*, Nucl. Instrum. and Meth. A 424 (1998) 444.
[30] B. Adeva *et al.*, Nucl. Instrum. Methods A 435 (1999) 402.
[31] A. Bressan *et al.*, Nucl. Instrum. and Meth. A424 (1998) 321.
[32] V. Peskov *et al.*, IEEE Trans. Nucl. Sci. NS-45 (1998) 244.
[33] P. Fonte *et al.*, Nucl. Instrum. and Meth. A 419 (1998) 405.
[34] G. Charpak *et al.*, Phys. Letters 78 B (1978) 523.
[35] R. Bouclier *et al.*, Nucl. Instrum. and Meth. A396 (1997) 50.
[36] T. Zeuner, Nucl. Instrum. Methods A 446 (2000) 324.
[37] C. Büttner *et al.*, Nucl. Instrum. and Meth. A 409 (1998) 79.
[38] A. Bressan *et al.*, Nucl. Instrum. and Meth. A425 (1999) 262.
[39] S. Bachmann *et al.*, IEEE Trans. Nucl. Sci. NS-47 (2000) .
[40] A. Buzulutskov *et al.*, Nucl. Instrum. and Meth. A433 (1998) 471.
[41] A. Buzulutskov *et al.*, Nucl. Instrum. Methods A 443 (2000) 164.